energies

MDPI

Article

Use of Carbon Additives towards Rechargeable Zinc Slurry Air Flow Batteries

Nak Heon Choi [1,2,*], Diego del Olmo [3], Diego Milian [4], Nadia El Kissi [4], Peter Fischer [1], Karsten Pinkwart [1,5] and Jens Tübke [1,2]

1 Applied Electrochemistry, Fraunhofer Institute for Chemical Technology ICT, Joseph-von-Fraunhofer, Straße 7, 76327 Pfinztal, Germany; peter.fischer@ict.fraunhofer.de (P.F.); karsten.pinkwart@ict.fraunhofer.de (K.P.); jens.tuebke@ict.fraunhofer.de (J.T.)
2 Institute for Mechanical Process Engineering and Mechanics, Karlsruhe Institute of Technology KIT, Straße am Forum 8, 76131 Karlsruhe, Germany
3 Department of Chemical Engineering, University of Chemistry and Technology Prague, Technická 5, 16628 Prague 6, Czech Republic; Diego1.Del.Olmo.Diaz@vscht.cz
4 CNRS, Grenoble INP, LRP, Institute of Engineering, Univ. Grenoble Alpes, LRP, 38000 Grenoble, France; diego.milian@univ-grenoble-alpes.fr (D.M.); nadia.elkissi@univ-grenoble-alpes.fr (N.E.K.)
5 Faculty of Electrical Engineering and Information Technology, Karlsruhe University of Applied Sciences, Moltkestraße 30, 76133 Karlsruhe, Germany
* Correspondence: nak.choi@ict.fraunhofer.de; Tel.: +49-721-4640-827

Received: 31 July 2020; Accepted: 20 August 2020; Published: 31 August 2020

Abstract: The performance of redox flow batteries is notably influenced by the electrolyte, especially in slurry-based flow batteries, as it serves as both an ionic conductive electrolyte and a flowing electrode. In this study, carbon additives were introduced to achieve a rechargeable zinc slurry flow battery by minimizing the zinc plating on the bipolar plate that occurs during charging. When no carbon additive was present in the zinc slurry, the discharge current density was 24 mA·cm^{-2} at 0.6 V, while the use of carbon additives increased it to up to 38 mA·cm^{-2}. The maximum power density was also increased from 16 mW·cm^{-2} to 23 mW·cm^{-2}. Moreover, the amount of zinc plated on the bipolar plate during charging decreased with increasing carbon content in the slurry. Rheological investigation revealed that the elastic modulus and yield stress are directly proportional to the carbon content in the slurry, which is beneficial for redox flow battery applications, but comes at the expense of an increase in viscosity (two-fold increase at 100 s^{-1}). These results show how the use of conductive additives can enhance the energy density of slurry-based flow batteries.

Keywords: zinc slurry air flow battery; redox flow battery; zinc-air battery; carbon additives; rheology

1. Introduction

Lately, the use of energy storage systems (ESS) to support renewable energies, like solar energy and wind energy, has attracted remarkable attention [1]. To achieve high energy densities for renewable energy, redox flow batteries (RFBs) are a promising candidate owing to their ability to decouple the control of energy capacity and power [2,3]. The energy densities of RFBs can be tuned by the capacity of electrolyte and the concentration of active species. On the other hand, the power density is determined by the electrode size and material. Different types of RFB systems are under investigation, such as vanadium-based, hydrogen-bromine, and organic RFB couples [4–6]. Using zinc as an active metal is very attractive, due to its abundance and low cost, including the electrolyte component, such as potassium hydroxide and zinc oxide [7,8]. Furthermore, zinc itself has a relatively high theoretical energy density (1350 Wh kg^{-1}) compared to other active materials [3]. Conventional zinc-air batteries consist of a positive compartment where air can flow in and out and a static porous zinc electrode in

the negative compartment [9,10]. On the other hand, the zinc slurry air flow battery uses a negative electrode with zinc particles suspended in a highly alkaline electrolyte (such as potassium hydroxide) with gelling agents forming a slurry, which can flow in and out of the cell [5]. The corresponding chemical reactions are presented below and a schematic diagram of this system configuration is shown in Figure 1. During discharge, the oxygen reduction reaction (ORR) occurs while zinc particles in the slurry oxidize to zincate, which can further decompose to zinc oxide in KOH, and the reactions are reversed when charging [11].

$$\text{Negative Electrode: } Zn + 4OH^- \leftrightarrow Zn(OH)_4^{2-} + 2e^- \text{ (E0 = −1.26 V)}$$

$$\text{Positive Electrode: } O_2 + 2H_2O + 4e^- \leftrightarrow 4OH^- \text{ (E0 = +0.40 V)}$$

$$\text{Electrolyte: } Zn(OH)_4^{2-} \leftrightarrow ZnO + H_2O + 2OH^-$$

$$\text{Overall: } 2Zn + O_2 \leftrightarrow 2ZnO \text{ (}\Delta\text{E0 = 1.66 V)}$$

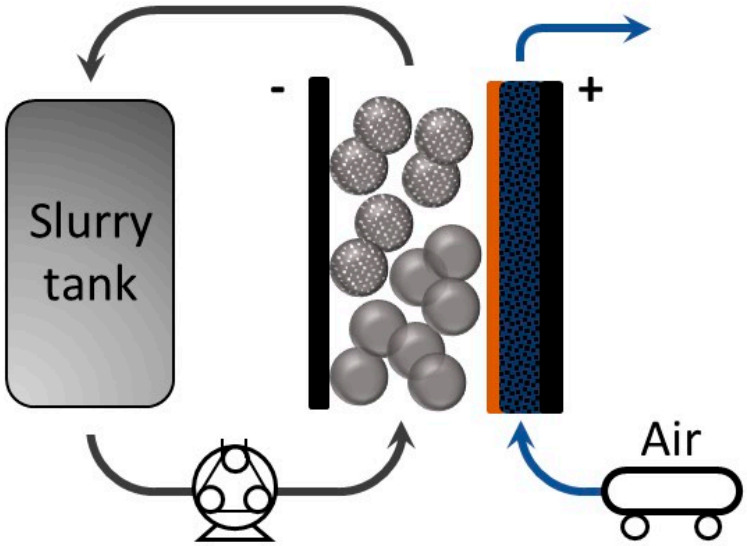

Figure 1. Schematic diagram of a zinc slurry air flow battery.

The capacity of conventional zinc-air batteries is determined by the size of the porous zinc electrode embedded in the system. However, for a zinc slurry air flow battery the capacity can be controlled by the amount of zinc in the slurry, independently of the cell size. Thus, the battery capacity can be tuned by varying the tank volume or the concentration of zinc particles in the slurry [12]. Another potential advantage of zinc slurry air flow batteries relates to the charging process. One of the main limitations of zinc-air batteries is dendrite growth on the zinc electrode, which will eventually pierce the membrane and result in a battery short-circuit. In the zinc slurry air flow battery, zinc plates on the bipolar plate or, preferably, on the zinc slurry, as there is no static porous electrode, such as carbon felts. Hence, this system configuration provides a space between the bipolar plate and membrane which helps prevent membrane damage when charging. Furthermore, it is reported that flowing configurations prevent the dendrites from growing perpendicular to the bipolar plate [13–16]. Nonetheless, as slurries are heterogeneous systems composed of non-soluble particles, there is a need to use gelling agents to prevent sedimentation and ensure a percolated network.

Gel polymer electrolytes (GPEs) are very interesting for zinc slurry air flow batteries, because advantages from both aqueous electrolytes and solid electrolytes can be encountered [17]. Depending on the battery design, the rheological behavior can be tuned up to favor cell efficiency by using carefully chosen gelling agents [18], rendering storage systems more flexible and adaptable to different scenarios [19]. Carbopol 940 (polyacrylic acid) has been recently investigated in different configurations

as conventional alkaline metal-air batteries like Al-air battery [20] and Zn-air batteries [21]. Moreover, polyacrylic acid (PAA) has been proven to show higher conductivity compared to other GPEs like PVA and PAM at 6 M KOH [22]. In this same study, rechargeability tests were performed with an efficiency of 79% at 0.5 mA cm^{-2}, and it was proved that charge transfer resistance was reduced by using GPEs. As a result of its mechanical properties (see J. M. Piau [23]), and chemical stability [22], PAA has already been used to formulate Zn slurries [5], and further investigations are being made to assess its performance as a gelling agent.

The use of electrolyte additives for improving the performance of non-flowing zinc-air batteries has also been widely investigated [24]. Furthermore, conductive additives (as graphite or carbon black) can be included in the formulation of Zn electrodes [25–28], leading to improved discharge capacities and power densities by increasing electronic conductivity, connectivity between Zn particles and providing nucleation sites for ZnO. Similarly, the use of carbon conductive additives for slurry redox flow batteries [29–33] and slurry capacitors [34,35] has also been investigated in the literature. Recently, Akuzum et al. [35] studied the use of three different carbon additives for a slurry capacitor—they concluded that the morphology of the additive plays an important role on the rheo-electric performance of the slurry electrode. Nonetheless, despite the use of carbon additives for zinc slurries has been proposed previously [36], its influence in the charging performance has not been investigated in detail.

Herein, we introduce carbon additives into a zinc slurry and study how the carbon additive affects both the charge and discharge performance of the zinc slurry air flow battery. Furthermore, using slurries with different carbon contents, we study the cycling performance and energy efficiency of the system. Finally, we show how the use of carbon additives reduces the amount of zinc plating onto the bipolar plate as zinc preferentially deposits in the carbon present in the slurry.

2. Materials and Methods

2.1. Air Electrode

The catalyst-coated electrode (CCE) approach was used to prepare the positive electrode. The catalyst ink consisted of a mixture of Pt black (Platinum black, Alfa Aesar, Kandel, Germany) and IrO_2 (99% Iridium oxide, Alfa Aesar, Kandel, Germany) with a ratio of 1:1 with 10 wt.% Fumion FAA-3 Ionomer (Fumatech, Bietigheim-Bissingen, Germany), deionized water, and isopropanol. The ink was first homogenized in an ultrasonic water bath for 10 min, and then again, using an ultrasonicator for another 10 min, to ensure a well-dispersed mixture. Then, the ink was manually sprayed onto a 25 cm^2 commercial gas diffusion layer (SGL Carbon, 29BC, Meitingen, Germany) with a spray gun. The platinum and iridium oxide loadings on the catalyst layer were fixed at 0.5 mg·cm^{-2} each, and the ionomer content was set to 23 wt.%.

2.2. Zinc Slurry Preparation

The base gel polymer electrolyte consists of 10 M KOH (Carl Roth, Karlsruhe, Germany) with Carbopol TM 940 (Acros Organics, Nidderau, Germany) as a gelling agent. To ensure a strong gel network, the GPE was mixed with a high shear homogenizer Yellow line, Ultra Turrax DI 25 basic (Ika, Staufen, Germany) at 9.500 rpm. Then, the zinc powder (GC 7-4/200 Bi/200ln, Grillo, Duisburg, Germany) with D_{50} = 55 µm, ZnO (VWR Chemicals, Dietikon, Switzerland), and carbon black (CB, carbon black, acetylene, 50% compressed, Alfa Aesar, Kandel, Germany) with D_{50} = 0.045 µm were added and the mixture was again homogenized for a total of 9 min. The slurry compositions are shown below in Table 1; note that the amount of the carbon black and 10 M KOH added up to 61.5 wt.%. The total volume of zinc slurry used for each experiment was approximately 70 mL.

Table 1. Composition of the zinc slurries.

	Mass Fraction (wt.%)				
	Zinc	**ZnO**	**Carbopol**	**Carbon Black**	**KOH + Water**
0 Carbon (0%CB)	33.8	4	0.7	0	61.5
0.2 Carbon (0.2%CB)				0.2	61.3
0.6 Carbon (0.6%CB)				0.6	60.9
1 Carbon (1%CB)				1	60.5

2.3. Cell Design and Electrochemical Characterization

The electrochemical characterization of the slurries was conducted using an in-house designed single cell presented in our previous study [5]. It comprises bipolar plates with a geometric active area of 25 cm^2, a separator, gaskets, and current collectors enclosed by two end plates. This is a single cell configuration, however, as it is focused on upscaling to a stacked design, the graphite plate at the negative electrode and metallic plate at the positive electrode are referred to as bipolar plates in this paper. As the charging voltage was higher than 2 V, the positive side bipolar plate was made of CuNi alloy, whereas the negative electrode bipolar plate was made of graphite to minimize zinc plating on it. The flow fields for both bipolar plates were serpentine as described in our previous study [5]. The CCE was placed between the positive-side bipolar plate and the porous membrane separator (Cellophane™ PØØ purchased from FUTAMURA, Hamburg, Germany).

The electrochemical performance of each slurry was studied by current-voltage characteristic curves (polarization curves) and galvanostatic cycling using a BaSyTec GSM Battery Test System (BaSyTec GmbH, Asselfingen, Germany). The galvanostatic cycling had a time stop-condition of 10 min per half-cycle and the voltage cut-offs were 0.3 V for discharge and 2.3 V for charge. The flow rates of active materials were 160 mL·min^{-1} for the zinc slurry in the negative compartment and 100 mL·min^{-1} for the synthetic air in the positive compartment. The voltage reported in the polarization curves was averaged over 30 s at each current density, due to the fluctuations caused by using a slurry electrode.

2.4. Rheometry

The rheology of the slurries was investigated by means of steady shear and oscillatory rheometry. A stress-controlled rheometer AR-G2 (TA instruments) equipped with a four-blade vane-in-cup geometry (L = 45.5 mm, D = 30 mm) was used to reduce flow-related heterogeneity issues [37,38]. The cup was equipped with a grill to reduce slippage effects [39]. This tool was calibrated following the procedure described by Baravian for large finite gaps [40]. All experiments were performed at room temperature.

The steady-state measurements were obtained by applying a constant shear rate from 100 to 0.01 s^{-1}. It was chosen to start from high shear rates to low shear rates to ensure viscosity steady-state measurements [41]. To quantify the rheological parameters of the carbon slurries, shear stress vs. shear rates curves were fitted to a Herschel-Bulkley model:

$$\tau = \tau_y + K\dot{\gamma}^n$$

where τ is the shear stress, τ_y is the yield stress, K is the consistency index, $\dot{\gamma}$ is the yield stress, and n is the flow index. Oscillatory strain amplitude sweep tests were carried from 0.1 to 1000% at 1 Hz to determine the linear viscoelastic region and both storage and loss moduli.

3. Results

Initial testing of the cycling behavior of our prototype zinc slurry air flow battery revealed that, during charging, part of the regenerated zinc was plated on the bipolar plate (see Figure 2a). The plating of metal on the bipolar plate is the working principle of flow-assisted batteries, such as zinc-nickel [42].

However, it is an undesired process for zinc slurry air flow batteries, as it limits the capacity of the system. In this situation, the maximum amount of zinc that can be recharged would be given by the size of the cell and depth of the channel rather than the total volume of slurry. Furthermore, the plated zinc can grow to form dendrites which could block the slurry flow and, eventually, break through the membrane producing a short circuit.

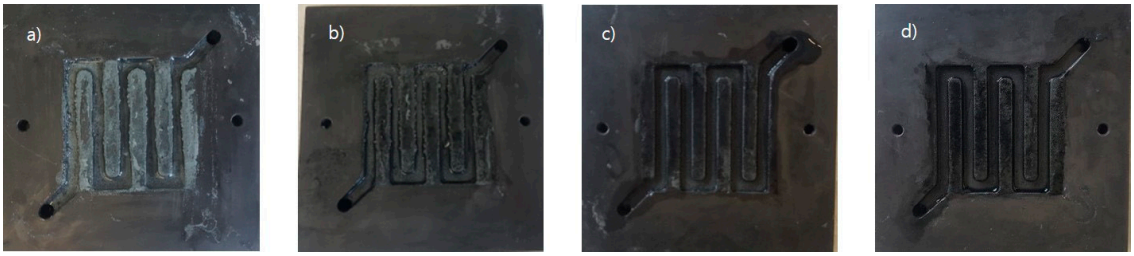

Figure 2. Zinc-side bipolar plate after charging: (**a**) 0% carbon black (CB), (**b**) 0.2% CB, (**c**) 0.6% CB, (**d**) 1% CB.

To try to mitigate this effect, we introduced carbon additives in the slurry aiming to shift the zinc plating from the bipolar to the carbon additive in the slurry. This new formulation would allow the recharged zinc to flow in and out of the system leading to a slurry flow battery configuration rather than a flow-assisted configuration. The suitability of the concept was evidenced by visual inspection of the bipolar plate after cycling slurries with different carbon contents. It can be seen in Figure 2 how the use of an increasing amount of carbon in the slurry led to lower zinc plating on the bipolar plate.

3.1. Oscillatory and Shear Rheometry

First, we determined the rheological behavior of the slurries under study, to assess their suitability for slurry RFBs. Oscillatory rheometry (Figure 3) revealed a linear viscoelastic region (LVR) where G'>>G", indicating that the total stress was given mostly by the elastic modulus G'. The LVR is characterized by a moduli plateau where viscoelastic properties do not depend on strain. This behavior was found in all samples indicating that a percolated network exists within the linear region [43].

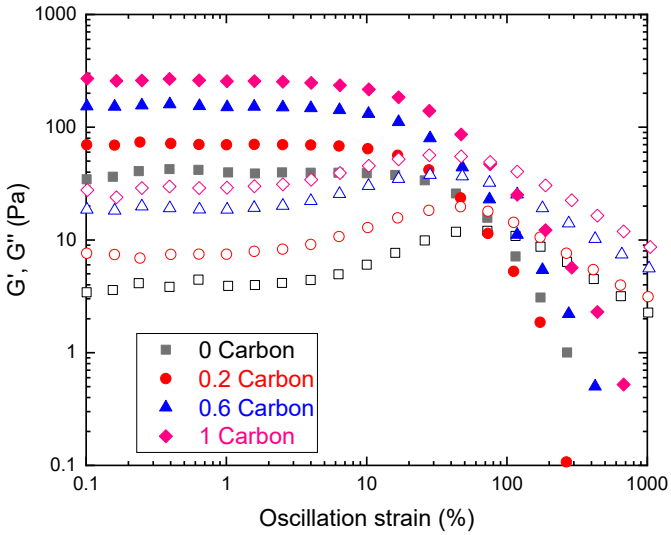

Figure 3. Oscillatory strain amplitude sweep test performed at f = 1 Hz for carbon slurries. Closed symbols represent storage moduli (G') and open symbols loss moduli (G").

As shown in Figure 3, higher carbon concentrations yielded higher moduli values, representing networks that tend to behave more as elastic solids, meaning that an optimal tradeoff between sample

structure and viscosity needs to be found. Another important characteristic of these curves is that, after a given strain, the moduli trend was reversed (G″ was greater than G′), indicating an inversion in the behavior as the sample breaks and starts to flow, indicating a yield stress [44]. As discussed in the latter reference, there is no standardized calculation of yield stress by oscillatory methods. Therefore, the yield stress of the slurries was determined using shear rheometry.

The steady-state measurements (Figure 4) showed that the slurries follow a non-Newtonian behavior, more specifically a shear thinning behavior. Such behavior proves beneficial to slurry-based RFBs as it reduces particle sedimentation and segregation at rest and viscosity decreases as the slurry is pumped. In general, the addition of CB led to a decrease in the flow index (see inset Figure 4b). Newtonian fluids have a flow index $n = 1$, while carbon slurries analyzed in this study follow a shear-thinning behavior ($n < 1$). The flow index increased when carbon was present, but at higher carbon concentrations, it decreased at values lower than the slurry without CB and shear thinning behavior is well established.

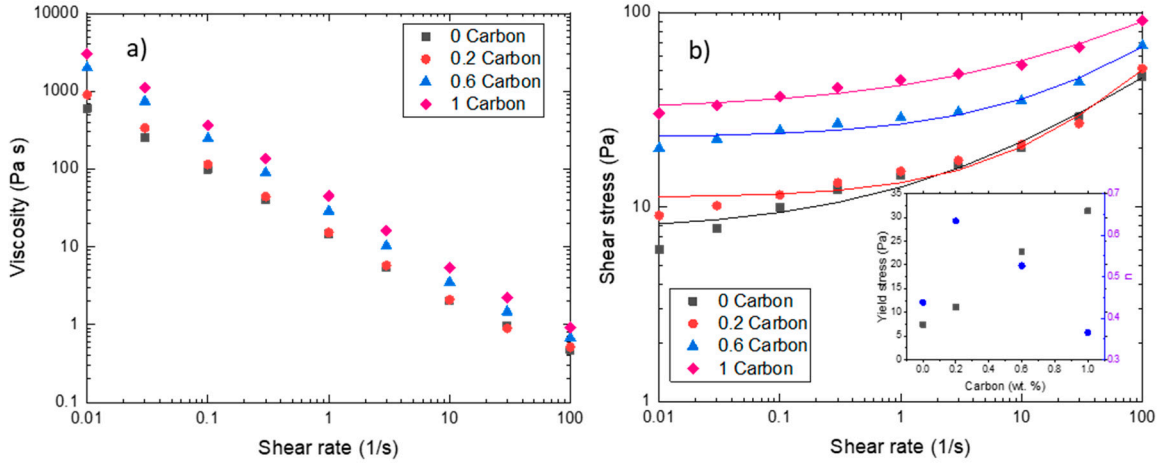

Figure 4. Steady-state rheometry. (**a**) Viscosity values vs. shear rate for carbon slurries. (**b**) Shear stress vs. shear rate for carbon slurries. Lines represents Herschel-Bulkley fitting. The inset in the graph shows the values of yield stress and flow index for all carbon slurries obtained from the fit.

In Figure 4a, we observe that the viscosity values decreased by a factor of 10^4 for 1%CB (highest CB concentration) and a factor of 10^3 for 0CB (lowest CB concentration) in the range of shear rates analyzed. The 0CB and 0.2%CB slurries showed similar values at high shear rates (from 0.1 s^{-1}), indicating that the addition of 0.2 wt.% of CB did not influence the viscosity, even if it modified its viscoelastic properties (Figure 3). For the slurries with higher CB contents, the addition of carbon black resulted in a five-fold viscosity increase for 1%CB at low shear rates and a two-fold increase at high shear rates. This is in agreement with the investigation performed by Gallier et al. [45], indicating that contact forces increase the shear stress because of the friction and roughness of particles close to each other, before entering a lubricational regime at higher shear rates where these contacts are reduced.

Figure 4b shows the shear stress as a function of shear rate. These slurries showed a yield stress behavior; thus, the data were fitted to a Herschel-Bulkley model. As discussed by Smith et al. [13], several rheological parameters can be tuned to improve the energy efficiency of the system, as yield stress. As seen in the inset of Figure 4b, carbon black concentration was directly proportional to yield stress. Wei et al. [43] have demonstrated that higher yield stresses lead to higher electronic conductivity, which is beneficial for the battery tested in this study. On the other hand, higher pressure drops must be attained to overcome yield stress which can severely affect the total efficiency of the system [46].

3.2. Polarization Curve Analysis

We then studied the influence of the carbon additive in the electrochemical performance of the system. The resulting polarization curves are shown in Figure 5. For discharge (Figure 5a),

it can be observed that, at low current densities, corresponding with the kinetic or activation region, the zinc slurries with carbon exhibited higher current densities than the one without. At 0.6 V, the current density of each slurry was 24 mA·cm^{-2} for 0CB, 38 mA·cm^{-2} for 0.2%CB, 36 mA·cm^{-2} for 0.6%CB, and 28 mA·cm^{-2} for 1%CB. The better electrochemical performance is attributed to stronger particle connectivity in the zinc slurry promoted by the carbon additive, which leads to a higher electrochemically active area (i.e., surface area of percolating zinc particles). However, at higher current densities, corresponding with the mass transfer limitation region, an increasing carbon content led to a decrease in electrochemical performance. The presence of carbon can difficult the access of OH^- to the zinc particles by blocking them (as they are smaller) which results in the mass transfer being hindered by the excess of carbon in the slurry. Nonetheless, the slurry with 0.2%CB still outperformed the one without additive over the whole range of current densities tested. Moreover, the maximum power density of the samples with CB was also higher. The measured values were 23 mW·cm^{-2} for 0.2%CB, followed by 22 mW·cm^{-2} for 0.6%CB, and 17 mW·cm^{-2} for 1%CB, whereas the zinc slurry with no carbon additive showed the lowest maximum power density of 16 mW cm^{-2}.

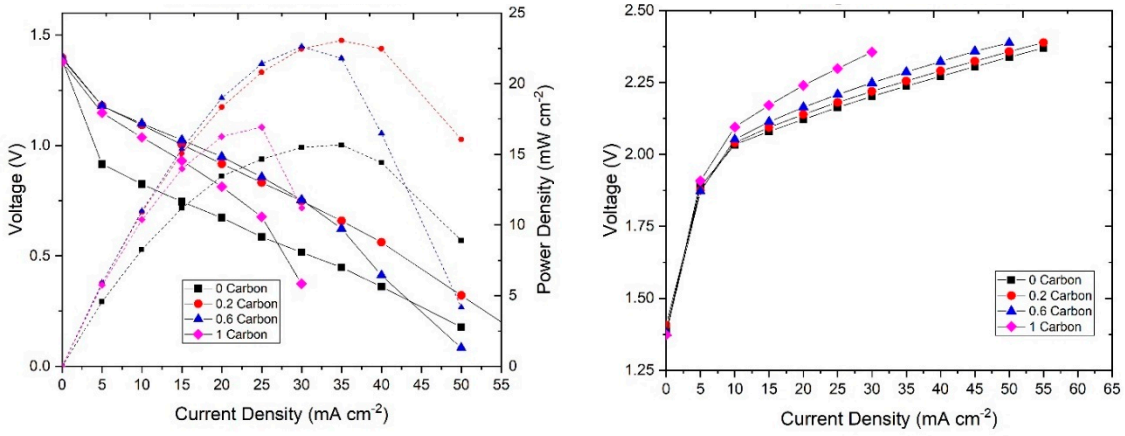

(**a**) (**b**)

Figure 5. (**a**) Discharge polarization curves with their power densities and (**b**) charge polarization of the zinc slurries with different carbon contents.

From the slopes of the polarization curves, we can observe that the ohmic resistance seems to increase with increasing carbon content. It should be noted that the ohmic resistance covers both the ionic and electronic resistance, which in slurry electrodes are comparable [47]. Therefore, the stronger network of particles in the slurry promoted by the carbon leads to better connectivity leading to lower electronic resistance. However, as the carbon content increases, the ionic resistance also increases as the volume fraction of electrolyte (equivalent to electrode porosity) decreases. Similarly, the intrinsic porosity of the carbon particles (i.e., pores inside the CB particles that can be filled with electrolyte) could further difficult the access of hydroxyl ions to the zinc particles. It can be also observed that more viscous slurries tend to increase the mass transfer resistance of the system.

Furthermore, the charging polarization curves (Figure 5b) show that an increase in carbon content leads to a lower charging performance. This can be, again, related to the increasing ohmic resistance given by the lower ionic conductivity. In this case, the charge transfer resistance of the zinc electrode does not seem to play a big role as in discharge, therefore, the higher electroactive area of the slurries with zinc particles does not influence the charge transfer polarization significantly.

3.3. Cycling Performance

Next, we studied the galvanostatic cycling performance of the slurries, the results are presented in Figure 6 below. All the slurries were successfully cycled at 10 mA·cm^{-2}, but at 20 mA·cm^{-2} the slurry

with 1%CB failed to complete the 10-min galvanostatic charge-discharge cycle, as it surpassed the charge cutoff voltage. Similarly, it can be noted that even at 10 mA·cm^{-2} the voltage of the 1%CB slurry during charge was higher than the rest, which agrees with the polarization results. The main reason for this was the decrease in ionic conductivity, as discussed previously. Moreover, it was observed during cycling that the slurries with high carbon contents (particularly 1%CB) were not able to flow smoothly into the cell leading to the presence of air bubbles in the channel. Such bubbles would reduce the effective active mass in the cell and, therefore, lead to the lower cycling performance.

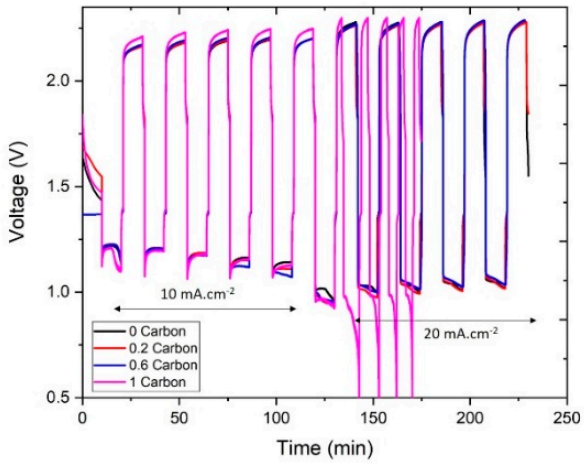

Figure 6. Charge-discharge curves of the different slurries.

On the other hand, the rest of the slurries presented a similar cycling behavior at both 10 and 20 mA·cm^{-2}. The energy efficiency of the 1st and 4th cycles at each current density is shown in Figure 7. At 10 mA·cm^{-2}, the energy efficiency in the 1st cycle was around 55% for all the samples, and it dropped to around 50% in the 4th cycle. At 20 mA·cm^{-2}, the slurry with no carbon showed a slightly higher energy efficiency (46%) compared to the slurries with carbon (43–44%) at the first cycle. After four cycles, the energy efficiency of the slurry with no carbon remained the same, while for the slurries with carbon it showed different trends: 0.2%CB dropped to 40% and 0.6%CB showed an increase to 47%. Note that the energy efficiency was limited by the high voltage difference between charge and discharge, rather than by the current efficiency.

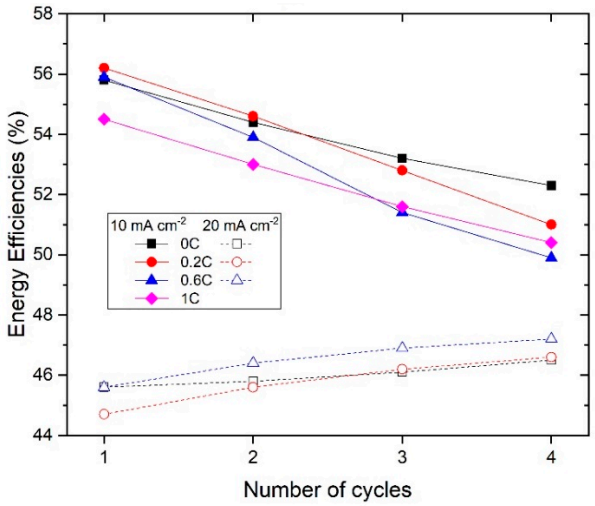

Figure 7. Energy efficiency of the different slurries.

3.4. Estimation of Charging Efficiency

To demonstrate that zinc plates preferentially on the carbon additive present in the slurry, further experiments were performed. First, each zinc slurry was charged for 20 min at 20 mA·cm^{-2}. Then, after the charge was completed, the zinc slurries were replaced by 10 KOH. This experiment aimed to estimate the discharge capacity of the zinc plated on the bipolar plate. It can be noted in Figure 8 that the discharge times were longer than the charge, leading to coulombic efficiencies over 100%. This is associated with two factors: (a) the existence of some dead volumes in the corners of the flow field could lead to remaining slurry present in the cell when discharging; (b) the zinc plated on the bipolar plate grows in uneven shapes, which could lead to zinc particles from the slurry being trapped into the plated zinc.

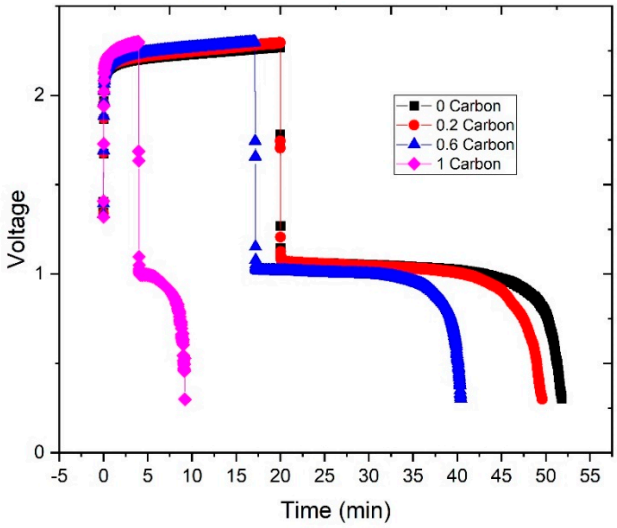

Figure 8. Charge-discharge curves to estimate zinc plating on the bipolar plate: charge with each zinc slurry and discharge after replacing the slurry with 10 M KOH.

From the curves in Figure 8 we can estimate the coulombic efficiency of the experiment, 0%CB showed the highest with 159%, then 148% for 0.2%CB, followed by 136% for 0.6%CB, and 132% for 1%CB. Unfortunately, due to the above-mentioned limitations, the experiment can only be taken as a qualitative measurement. Nonetheless, higher carbon contents led to shorter discharge times with KOH circulating through the cell, which can be associated with less zinc plating on the bipolar plate (as shown in Figure 2).

To avoid the effects leading to "over-efficient" charges, two slurries without zinc particles were prepared and tested. The new samples consist of the base electrolyte (10 M KOH, Carbopol and zinc oxide) with 1 wt.% and 2 wt.% of carbon, note that the volume fraction of solids in these samples is much lower than in the zinc slurries. As opposed to the previous cycling experiments, the new slurries must be charged first: they cannot be directly discharged as they contain no zinc particles. The results of the cycling tests are shown in Figure 9.

As shown in Figure 9, both slurries with 1 wt.% and 2 wt.% carbon could be cycled at 10 mA·cm^{-2}. However, at 20 mA·cm^{-2}, only the slurry with 2 wt.% of carbon was able to charge and discharge as 1 wt.% surpassed the experimental charging cut-off voltage (which leads to the premature termination of the experiment). With 2 wt.% of carbon, at 10 mA·cm^{-2}, charging voltage is lower than 1 wt.% carbon, which leads to stable charge-discharge performance at 20 mA·cm^{-2}. The coulombic efficiency at 20 mA·cm^{-2} of the slurry with 2 wt.% carbon was 89%, which suggests that hydrogen evolution was occurring as a side reaction (due to the low voltage in the negative electrode). To prove that the zinc was charging on the carbon particles in the slurry not on the bipolar plate, with 2 wt.% carbon, after the last charge the slurry was removed and 10 M KOH was circulated and discharged. The coulombic

efficiency, in this case, was only 4%, which confirms that there was almost no zinc plating on the bipolar when charging.

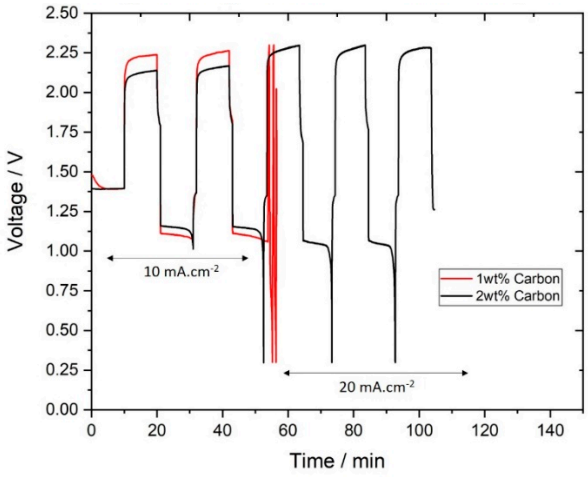

Figure 9. Charge-discharge curves of slurries without zinc particles.

4. Conclusions

In conclusion, slurries with different ratios of carbon additives were introduced to enhance the performance of zinc slurry air flow batteries aiming to prevent zinc plating on the bipolar plate when charging. The rheology of zinc-carbon slurries was analyzed revealing that, despite higher viscosity values, higher carbon contents also led to stronger networks characterized by higher storage moduli values and yield stresses that are beneficial to RFBs. Although the zinc slurry without carbon additives shows relatively stable performances for both charging and discharging, it was found that zinc plated on the bipolar plate during charge. On the other hand, when carbon was added to the zinc slurry, the discharge power density of the system was enhanced and the zinc plating during charge was shifted from the bipolar to the carbon additive in the slurry. This was proved by charge-discharge experiments using carbon slurries without zinc particles. When the zinc plating is shifted from the bipolar plate to the carbon additives in the slurry, a higher total battery capacity can be achieved.

Author Contributions: Conceptualization, N.H.C., D.d.O. and P.F.; Methodology, N.H.C. and D.M.; Software, D.d.O.; Writing—original draft preparation, N.H.C.; Resources, N.H.C. and D.M.; Writing—review and editing, N.H.C., D.d.O., D.M., N.E.K. and P.F.; Supervision, P.F., K.P. and J.T. All authors have read and agreed to the published version of the manuscript.

Funding: This project has received funding from the European Union's Horizon 2020 research and innovation programme under the Marie Skłodowska-Curie Grant Agreement no. 765289.

Conflicts of Interest: The authors declare no conflict of interest.

References

1. Sperstad, I.B.; Korpås, M. Energy Storage Scheduling in Distribution Systems Considering Wind and Photovoltaic Generation Uncertainties. *Energies* **2019**, *12*, 1231. [CrossRef]
2. Ding, Y.; Zhang, C.; Zhang, L.; Zhou, Y.; Yu, G. Pathways to Widespread Applications: Development of Redox Flow Batteries Based on New Chemistries. *Chem* **2019**, *5*, 1964–1987. [CrossRef]
3. Caramia, V.; Bozzini, B. Materials science aspects of zinc-air batteries: A review. *Mater. Renew. Sustain. Energy* **2014**, *3*, 28. [CrossRef]
4. Gentil, S.; Reynard, D.; Girault, H.H. Aqueous organic and redox-mediated redox flow batteries: A review. *Curr. Opin. Electrochem.* **2020**, *21*, 7–13. [CrossRef]
5. Choi, N.H.; del Olmo, D.; Fischer, P.; Karsten, P.; Tübke, J. Development of flow fields for Zinc Slurry Air Flow Batteries. *Batteries* **2020**, *6*, 15. [CrossRef]

6. Bockelmann, M.; Kunz, U.; Turek, T. Electrically rechargeable zinc-oxygen flow battery with high power density. *Electrochem. Commun.* **2016**, *69*, 24–27. [CrossRef]
7. Jiratchayamaethasakul, C.; Srijaroenpramong, N.; Bunyangyuen, T.; Arpavate, W.; Wongyao, N.; Therdthianwong, A.; Therdthianwong, S. Effects of anode orientation and flow channel design on performance of refuelable zinc-air fuel cells. *J. Appl. Electrochem.* **2014**, *44*, 1205–1218. [CrossRef]
8. Li, Y.; Gong, M.; Liang, Y.; Feng, J.; Kim, J.-E.; Wang, H.; Hong, G.; Zhang, B.; Dai, H. Advanced zinc-air batteries based on high-performance hybrid electrocatalysts. *Nat. Commun.* **2013**, *4*, 1–7. [CrossRef] [PubMed]
9. Zelger, C.; Süßenbacher, M.; Laskos, A.; Gollas, B. State of charge indicators for alkaline zinc-air redox flow batteries. *J. Power Sources* **2019**, *424*, 76–81. [CrossRef]
10. Wang, K.; Yu, J. Lifetime simulation of rechargeable zinc-air battery based on electrode aging. *J. Energy Storage* **2020**, *28*, 101191. [CrossRef]
11. Mainar, A.; Iruin, E.; Colmenares, L.; Blázquez, J.; Grande, H.-J. Systematic cycle life assessment of a secondary zinc–air battery as a function of the alkaline electrolyte composition. *Energy Sci. Eng.* **2018**, *6*, 174–186. [CrossRef]
12. Ma, H.; Wang, B.; Fan, Y.; Hong, W. Development and Characterization of an Electrically Rechargeable Zinc-Air Battery Stack. *Energies* **2014**, *7*, 6548–6557. [CrossRef]
13. Fu, J.; Cano, Z.P.; Park, M.G.; Yu, A.; Fowler, M.; Chen, Z. Electrically Rechargeable Zinc-Air Batteries: Progress Challenges and Perspectives. *Adv. Mater.* **2016**, *29*, 1604685. [CrossRef] [PubMed]
14. Aremu, E.O.; Park, D.J.; Ryu, K.S. The effects of anode additives towards suppressing dendrite growth and hydrogen gas evolution reaction in Zn-air secondary batteries. *Ionics* **2019**, *25*, 4197–4207. [CrossRef]
15. Zhao, Z.; Fan, X.; Ding, J.; Hu, W.; Zhong, C.; Lu, J. Challengis in Zinc Electrodes for Alkaline Zinc-Air Batteries: Obstacles to commercialization. *ACS Energy Lett.* **2019**, *4*, 2259–2270. [CrossRef]
16. Wang, K.; Pei, P.; Ma, Z.; Chen, H.; Xu, H.; Chen, D.; Wang, X. Dendrite growth in the recharging process of zinc-air batteries. *J. Mater. Chem. A* **2015**, *3*, 22648–22655. [CrossRef]
17. Liang, S.; Yan, W.; Wu, X.; Zhang, Y.; Zhu, Y.; Wang, H.; Wu, Y. Gel polymer electrolytes for lithium ion batteries: Fabrication, characterization and performance. *Solid State Ion.* **2018**, *318*, 2–18. [CrossRef]
18. Smith, K.C.; Chiang, Y.-M.; Carter, W.C. Maximizing Energetic Efficiency in Flow Batteries Utilizing Non-Newtonian Fluids. *J. Electrochem. Soc.* **2014**, *161*, A486–A496. [CrossRef]
19. Cheng, X.; Pan, J.; Zhao, Y.; Liao, M.; Peng, H. Gel Polymer Electrolytes for Electrochemical Energy Storage. *Adv. Energy Mater.* **2018**, *8*, 1702184. [CrossRef]
20. Zhang, Z.; Zuo, C.; Liu, Z.; Yu, Y.; Zuo, Y.; Song, Y. All-solid-state Al-air batteries with polymer alkaline gel electrolyte. *J. Power Sources* **2014**, *251*, 470–475. [CrossRef]
21. Lee, S.M.; Kim, Y.J.; Eom, S.W.; Choi, N.S.; Kim, K.W.; Cho, S.B. Improvement in self-discharge of Zn anode by applying surface modification for Zn-air batteries with high energy density. *J. Power Sources* **2013**, *227*, 177–184. [CrossRef]
22. Tran, T.N.T.; Chung, H.J.; Ivey, D.G. A study of alkaline gel polymer electrolytes for rechargeable zinc–air batteries. *Electrochim. Acta* **2019**, *327*, 135021. [CrossRef]
23. Piau, J.M. Carbopol gels: Elastoviscoplastic and slippery glasses made of individual swollen sponges. Meso- and macroscopic properties, constitutive equations and scaling laws. *J. Nonnewton. Fluid Mech.* **2007**, *144*, 1–29. [CrossRef]
24. Mainar, A.R.; Leonet, O.; Bengoechea, M.; Boyano, I.; de Meatza, I.; Kvasha, A.; Alberto Blázquez, J. Alkaline aqueous electrolytes for secondary zinc-air batteries: An overview. *Int. J. Energy Res.* **2016**, *40*, 1032–1049. [CrossRef]
25. Othman, R.; Yahaya, A.H.; Arof, A.K. A zinc-air cell employing a porous zinc electrode fabricated from zinc-graphite-natural biodegradable polymer paste. *J. Appl. Electrochem.* **2002**, *32*, 1347–1353. [CrossRef]
26. Masri, M.N.; Mohamad, A.A. Effect of adding carbon black to a porous zinc anode in a zinc-air battery. *J. Electrochem. Soc.* **2013**, *160*, A715. [CrossRef]
27. Tao, H.; Tong, X.; Gan, L.; Zhang, S.; Zhang, X.; Liu, X. Effect of adding various carbon additives to porous zinc anode in rechargeable hybrid aqueous battery. *J. Alloys Compd.* **2016**, *658*, 119–124. [CrossRef]
28. Chotipanich, J.; Arpornwichanop, A.; Yonezawa, T.; Kheawhom, S. Electronic and ionic conductivities enhancement of zinc anode for flexible printed zinc-air battery. *Eng. J.* **2018**, *22*, 47–57. [CrossRef]
29. Duduta, M.; Ho, B.; Wood, V.C.; Limthongkul, P.; Brunini, V.E.; Carter, W.C.; Chiang, Y.-M. Semi-Solid Lithium Rechargeable Flow Battery. *Adv. Energy Mater.* **2011**, *1*, 511–516. [CrossRef]

30. Youssry, M.; Madec, L.; Soudan, P.; Cerbelaud, M.; Guyomard, D.; Lestriez, B. Non-aqueous carbon black suspensions for lithium-based redox flow batteries: Rheology and simultaneous rheo-electrical behavior. *Phys. Chem. Chem. Phys.* **2013**, *15*, 14476–14486. [CrossRef]
31. Youssry, M.; Madec, L.; Soudan, P.; Cerbelaud, M.; Guyomard, D.; Lestriez, B. Formulation of flowable anolyte for redox flow batteries: Rheo-electrical study. *J. Power Sources* **2015**, *274*, 424–431. [CrossRef]
32. Shukla, G.; del Olmo Diaz, D.; Thangavel, V.; Franco, A.A. Self-Organization of Electroactive Suspensions in Discharging Slurry Batteries: A Mesoscale Modeling Investigation. *ACS Appl. Mater. Interfaces* **2017**, *9*, 17882–17889. [CrossRef] [PubMed]
33. Shukla, G.; Franco, A.A. Handling Complexity of Semi-solid Redox Flow Battery Operation Principles Through Mechanistic Simulations. *J. Phys. Chem.* **2018**, *122*, 23867–23877.
34. Hoyt, N.C.; Wainright, J.S.; Savinell, R.F. Current Density Scaling in Electrochemical Flow Capacitors. *J. Electrochem. Soc.* **2015**, *162*, A1102–A1110. [CrossRef]
35. Akuzum, B.; Singh, P.; Eichfeld, D.A.; Agartan, L.; Uzun, S.; Gogotsi, Y.; Kumbur, E.C. Percolation Characteristics of Conductive Additives for Capacitive Flowable (Semi-Solid) Electrodes. *ACS Appl. Mater. Interfaces* **2020**, *12*, 5866–5875. [CrossRef]
36. Kisdarjono, H.; Lu, Y.; Lee, J.-J.; Evans, D.; Wang, L. Air Cathode Battery Using Zinc Slurry Anode with Carbon Additive. Available online: https://patents.google.com/patent/US20140370401A1/en (accessed on 1 July 2020).
37. Hreiz, R.; Adouani, N.; Fünfschilling, D.; Marchal, P.; Pons, M.N. Rheological characterization of raw and anaerobically digested cow slurry. *Chem. Eng. Res. Des.* **2017**, *119*, 47–57. [CrossRef]
38. Hermoso, J.; Jofore, B.D.; Martínez-Boza, F.J.; Gallegos, C. High pressure mixing rheology of drilling fluids. *Ind. Eng. Chem. Res.* **2012**, *51*, 14399–14407. [CrossRef]
39. Owens, C.E.; Hart, A.J.; McKinley, G.H. Improved rheometry of yield stress fluids using bespoke fractal 3D printed vanes. *J. Rheol.* **2020**, *64*, 643–662. [CrossRef]
40. Baravian, C.; Lalante, A.; Parker, A. Vane rheometry with a large, finite gap. *Appl. Rheol.* **2002**, *12*, 81–87. [CrossRef]
41. Helal, A.; Divoux, T.; McKinley, G.H. Simultaneous Rheoelectric Measurements of Strongly Conductive Complex Fluids. *Phys. Rev. Appl.* **2016**, *6*, 064004. [CrossRef]
42. Ito, Y.; Nyce, M.; Plivelich, R.; Klein, M.; Steingart, D.; Banerjee, S. Zinc morphology in zinc–nickel flow assisted batteries and impact on performance. *J. Power Sources* **2011**, *196*, 2340–2345. [CrossRef]
43. Wei, T.S.; Fan, F.Y.; Helal, A.; Smith, K.C.; McKinley, G.H.; Chiang, Y.M.; Lewis, J.A. Biphasic Electrode Suspensions for Li-Ion Semi-solid Flow Cells with High Energy Density, Fast Charge Transport, and Low-Dissipation Flow. *Adv. Energy Mater.* **2015**, *5*, 1500535. [CrossRef]
44. Dinkgreve, M.; Paredes, J.; Denn, M.M.; Bonn, D. On different ways of measuring 'the' yield stress. *J. Nonnewton. Fluid Mech.* **2016**, *238*, 233–241. [CrossRef]
45. Gallier, S.; Lemaire, E.; Peters, F.; Lobry, L. Rheology of sheared suspensions of rough frictional particles. *J. Fluid Mech.* **2014**, *757*, 514–549. [CrossRef]
46. Tang, A.; Bao, J.; Skyllas-Kazacos, M. Studies on pressure losses and flow rate optimization in vanadium redox flow battery. *J. Power Sources* **2014**, *248*, 154–162. [CrossRef]
47. Petek, T.J.; Hoyt, N.C.; Savinell, R.F.; Wainright, J.S. Characterizing Slurry Electrodes Using Electrochemical Impedance Spectroscopy. *J. Electrochem. Soc.* **2015**, *163*, A5001–A5009. [CrossRef]